nature communications

Article

https://doi.org/10.1038/s41467-024-51745-4

# A single-domain antibody targeting factor XII inhibits both thrombosis and inflammation

Received: 25 November 2020

Accepted: 16 August 2024

Published online: 12 September 2024

Check for updates

Pengfei Xu[1,14], Yingjie Zhang[1,14], Junyan Guo[1,2], Huihui Li[1], Sandra Konrath[3], Peng Zhou[4], Liming Cai[5], Haojie Rao[1], Hong Chen[1], Jian Lin[4], Zhao Cui[6], Bingyang Ji[5], Jianwei Wang[7], Nailin Li[8], De-Pei Liu[9], Thomas Renné[3,10,11] & Miao Wang[1,12,13]

Factor XII (FXII) is the zymogen of the plasma protease FXIIa that activates the intrinsic coagulation pathway and the kallikrein kinin-system. The role of FXII in inflammation has been obscure. Here, we report a single-domain antibody (nanobody, Nb) fused to the Fc region of a human immunoglobulin (Nb-Fc) that recognizes FXII in a conformation-dependent manner and interferes with FXIIa formation. Nb-Fc treatment inhibited arterial thrombosis in male mice without affecting hemostasis. In a mouse model of extracorporeal membrane oxygenation (ECMO), FXII inhibition or knockout reduced thrombus deposition on oxygenator membranes and systemic microvascular thrombi. ECMO increased circulating levels of D-dimer, alkaline phosphatase, creatinine and TNF-α and triggered microvascular neutrophil adherence, platelet aggregation and their interaction, which were substantially attenuated by FXII blockade. Both Nb-Fc treatment and FXII knockout markedly ameliorated immune complex-induced local vasculitis and anti-neutrophil cytoplasmic antibody-induced systemic vasculitis, consistent with selectively suppressed neutrophil migration. In human blood microfluidic analysis, Nb-Fc treatment prevented collagen-induced fibrin deposition and neutrophil adhesion/activation. Thus, FXII is an important mediator of inflammatory responses in vasculitis and ECMO, and Nb-Fc provides a promising approach to alleviate thrombo-inflammatory disorders.

Thrombosis and inflammation are distinct biological processes that are closely interconnected in a broad variety of vascular diseases. Factor XII (FXII) initiates the contact activation pathway in plasma leading to the formation of thrombin and bradykinin (BK). Upon contact with negatively charged surfaces, FXII, which circulates in plasma as a zymogen, is activated and converted to the serine protease FXIIa. FXIIa acts as a procoagulant and proinflammatory mediator by triggering the intrinsic coagulation cascade and the kallikrein-kinin system, respectively. The latter involves the release of the vasoactive nonapeptide BK from high-molecular-weight kininogen after FXIIa-induced activation of plasma prekallikrein (PK). The structure of FXIIa comprises two chains, referred to as the heavy chain and the light chain. While the light chain harbors the catalytic triad of the protease (His393, Asp442, Ser544), the heavy chain is composed of the fibronectin type 1 and 2 domains (FnI and FnII), two epidermal growth factor domains (EGF1 and EGF2), a Kringle domain and a proline-rich region (PRR)[1,2]. Genetic deletion of *F12*[3,4] or inhibition of FXIIa activity using antibodies[5–8], protein/peptide inhibitors[8,9], or antisense

A full list of affiliations appears at the end of the paper. e-mail: miao.wang@pumc.edu.cn

oligonucleotides[10] provides thrombo-protection without affecting hemostasis in animal models. Hence, FXII has become a promising target for therapeutic and prophylactic interference with thrombosis[11].

In addition to its function in thrombosis, FXII has been shown to play a role in inflammatory responses[1]. For example, a missense mutation affecting threonine at position 309 within the PRR results in the loss of glycosylation at this site and an increased susceptibility to surface-mediated autoactivation of FXII[12]. This FXII gain-of-function mutation is associated with an excessive production of BK, which in turn mediates a rare swelling disorder, known as hereditary angioedema (FXII-HAE). In addition to hepatocytes, neutrophils also express FXII. Loss of neutrophil-derived FXII promotes wound healing via suppressing uPAR-Akt2 signaling[13]. Furthermore, FXII exaggerates CD4 T effector cell responses during neuroinflammation via modulation of dendritic cells[14]. Targeting FXIIa for interference with thrombosis is well established. However, the implications of FXII inhibition to interfere with inflammatory responses are poorly understood.

Nanobodies are recombinant, single-domain antigen-binding fragments, derived from variable fragments of heavy chain–only antibodies that naturally occur in camelids[15]. With a molecular weight of only 12–15 kDa, nanobodies, also known as VHH (variable heavy domain of a heavy-chain antibody), are the smallest functional antigen-binding fragments. A nanobody is similar in structure to that of a human heavy chain variable domain (VH), with major differences found in the framework 2 region and in the complementarity determining regions (CDRs)[16,17]. In particular, the third hypervariable loop (CDR3) of VHH domains is often significantly longer than that observed in human VH domains. CDR3 loops of VHHs usually fold across the region normally at the interface with the variable region of light chain in conventional antibodies[16,17], allowing them to recognize epitopes that are inaccessible to conventional antibodies[18]. Due to their small size, nanobodies are easier to engineer and have high stability. Nanobody-based drugs have recently been approved[19]. In this study, we designed a nanobody recognizing FXII and show its anti-inflammatory and anti-thrombotic efficacy in predictive experimental animal models with implications for human disease.

## Results

### Generation and characterization of a nanobody and its bivalent construct against human FXII

After immunizing an alpaca with human FXII (Supplementary Fig. 1), we constructed an immune library of VHHs from the animal's peripheral blood lymphocytes in a phage display vector. The VHH library contained ~$2.4 \times 10^8$ clones, of which more than 90% were estimated to contain a display vector with a VHH-sized insert. Twenty randomly selected clones were sequenced. These clones were found to have their VHH insert in frame and showed a large sequence diversity in their CDRs. After expression of the VHHs at the tip of M13 phage particles and five rounds of biopanning against human FXII (Fig. 1a), 26 clones with unique VHH sequences that specifically recognize FXII were obtained. Eighteen sequences were successfully expressed in *E. Coli* BL21, which showed a discernible VHH band on reducing SDS-PAGE. The corresponding recombinant proteins were purified (Supplementary Fig. 2). One product (Nb) that showed high binding affinity and neutralizing activity against FXII activation (Supplementary Figs. 3 and 4) was chosen for further study.

Nb (~13 kDa) and its bivalent construct (Nb-Fc, ~96 kDa), derived by fusion with an Fc segment of human immunoglobulin G4, were expressed in bacteria and CHO cells, respectively, and purified by affinity chromatography and characterized by Western blotting (Fig. 1b). The binding affinity of Nb and Nb-Fc for plasma-derived human FXII, indicated by the equilibrium dissociation constant (KD), was 3.26 nM and 0.41 nM, respectively (Fig. 1c). Dot blot hybridization was performed with native FXII or denatured FXII (heated at 100 °C for 10 min with 100 mM DTT). The binding affinity of Nb was markedly reduced when the denatured FXII was used, whereas incubation of Nb at 100 °C for 10 min did not affect its binding to native FXII (Fig. 1d). This indicates a conformational dependence of the FXII-binding epitope and a high refolding capacity of Nb after heat stress. The melting temperature of Nb, determined by circular dichroism, was 74.81 °C, suggesting a high thermostability. To further characterize the binding epitope of FXII, individual domains of FXII (the corresponding DNA sequences in Supplementary Table 1) were recombinantly expressed in bacteria and the reduced samples were used for antibody binding analysis by Western blotting. Nb only recognized single FnII and Kringle domains (Fig. 1e). These two domains are close to each other on a predicted three-dimensional structure from the AlphaFold Protein Structure Database (Supplementary Fig. 5). To confirm the Nb epitope, we used recently described HEK293 cell-derived FXII deletion mutants, which are deficient in single domains or regions[20]. Nb was unable to detect FXII and it deletion mutants under reducing conditions. The FXII variant lacking the Kringle domain (ΔKringle) was not detectable by Nb under non-reducing conditions. The data confirm a role of the Kringle domain in Nb binding in the context of an intact heavy chain. However, the FXII mutant deficient in FnII (ΔFnII) was detectable by Nb (Fig. 1f), highlighting the conformational dependence of the Nb epitope. The data indicate potentially different structures of the individual GST-fused FnII domain and the respective domain in an intact heavy chain and/or different strengths of Nb binding to FnII vs. Kringle domains. Activation of FXII and PK was then examined in vitro using the chromogenic substrates S-2302 and CS-31(02). Ellagic acid (EA), polyphosphate (polyP) and dextran sulfate (DXS) were used to trigger FXII activation (Supplementary Fig. 6a–c). Nb dose-dependently inhibited EA-, polyP- or DXS-induced activation of FXII (Supplementary Fig. 6d–f). Nb did not inhibit FXIIa (Supplementary Fig. 6g). Hence, Nb inhibited contact-driven FXII activation but did not directly interfere with the protease activity of the activated FXII. An isotype control antibody of Nb-Fc (Iso-Fc) was similarly generated by expression in CHO cells, with the CDR regions removed from Nb-Fc (Supplementary Fig. 6h). Similar to Nb, Nb-Fc also dose-dependently inhibited EA-induced activation of FXII and plasma kallikrein formation, with an IC50 of ~13 μg/mL (Fig. 1g, h). Furthermore, Nb-Fc prolonged human plasma activated partial thromboplastin time (aPTT) in a dose-dependent manner (Fig. 1i). Notably, the presence of Nb had no effect on the prothrombin time (PT, a measure of the tissue factor-initiated extrinsic coagulation pathway) (Supplementary Fig. 6i), indicating its specificity for targeting the intrinsic pathway of coagulation. Nb also cross-reacted with mouse FXII (KD = 25.0 nM) (Supplementary Fig. 7a), and Nb-Fc inhibited EA-induced activation of mouse FXII (Supplementary Fig. 7b). The half-life of Nb-Fc was >14 d in mice (Supplementary Fig. 8).

### Nb-Fc inhibits thrombosis without affecting hemostasis

The effect of Nb-Fc on thrombosis was evaluated in a mouse model of carotid artery thrombosis induced by ferric chloride ($FeCl_3$). The newly constructed FXII-deficient (*F12*$^{-/-}$) mice[21], which have prolonged aPTT (Supplementary Fig. 9) and unaltered activated clotting time (ACT) (Supplementary Fig. 10), were used as positive control. Nb-Fc treatment prolonged the time to complete occlusion and reduced occlusion rates in a dose-dependent manner, with comparable results observed between a 10 mg/kg dose of Nb-Fc and FXII deficiency (Fig. 2a). Nb-Fc also inhibited cremaster muscle arteriolar thrombosis at a low dose (1 mg/kg) as assessed with intravital microscopy (Fig. 2b, c). Nb-Fc treatment did not alter tail bleeding time (Fig. 2d). Thus, Nb-Fc efficiently inhibits thrombosis without affecting hemostasis in rodents, confirming its specificity for targeting FXII.

### Nb-Fc attenuates ECMO-related thromboinflammation and organ injury in mice

Extracorporeal membrane oxygenation (ECMO) is used to support patients with severe cardiocirculatory and/or respiratory failure by

https://doi.org/10.1038/s41467-024-51745-4

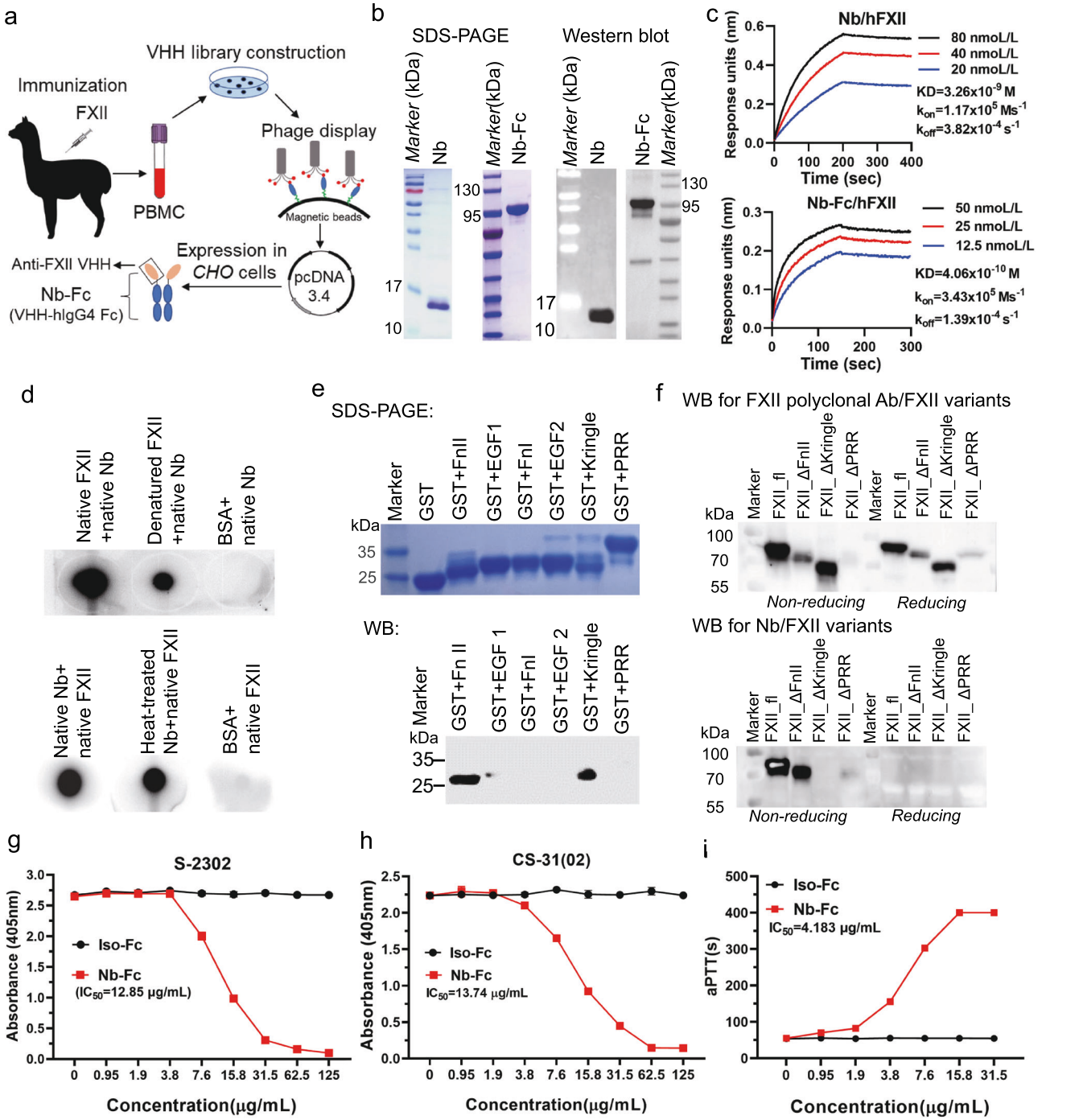


**Fig. 1 | Generation and characterization of FXII-specific nanobody (Nb) and its Fc construct variant fused to the Fc of human immunoglobulin G4 (Nb-Fc).** **a** Schematic representation of the strategy used to identify FXII-specific nanobodies and to design nanobody-Fc fusion after immunizing an alpaca with human FXII. **b** Characterization of *E. coli* BL21-expressed Nb and Chinese Hamster Ovary (CHO) cell-expressed Nb-Fc by SDS-PAGE (left panel) and Western blot (right panel). **c** Binding affinity of Nb or Nb-Fc to human FXII determined by kinetic assays using the Fortebio Octet System. **d** Dot blot assay to analyze the interaction of native or heat-treated FXII and Nb as indicated. BSA was used as control. **e**, **f** FXII epitope mapping. **e** FXII domains were individually expressed using *E. coli* BL21, separated by SDS-PAGE under reducing conditions and visualized by Brilliant Coomassie Blue (upper panel), and probed for Nb binding by Western blot (lower panel). **f** Full-length FXII (FXII_fl) and FXII mutants with indicated deleted domains (FXII_ΔFnII: deletion of FnII; FXII_ΔKringle: deletion of the Kringle domain; FXII_ΔPRR: deletion of the C-terminal part of PRR) were expressed in HEK 293 cells. Binding capacity of a polyclonal anti-FXII antibody as control (upper panel) and Nb (lower panel) to the mutants was evaluated by Western blot under both reducing and non-reducing conditions. **g** Effects of increasing concentrations of Nb-Fc on ellagic acid (EA, 4 μg/ml)-induced FXII activation using the FXIIa-specific substrate S-2302 (final concentration: 0.8 mM). Isotype control antibody (Iso-Fc) was used as control. **h** Effects of Nb-Fc on plasma prekallikrein (PK) activation. FXII was pre-treated with Nb-Fc, followed by the addition of EA (final concentration: 4 μg/mL) and PK (6.25 μg/mL), then the chromogenic substrate CS-31(02) was used to evaluate the enzymatic activity of activated PK. **i** Effects of Nb-Fc on activated partial thromboplastin time (aPTT). Citrated human plasma was incubated with increasing concentrations of Nb-Fc (0–31.5 μg/ml) for 5 min prior to aPTT measurements. Experiments in **b**, **d**–**f** were independently performed twice with consistent results. See the Methods for details. Source data are provided as a Source Data file.

https://doi.org/10.1038/s41467-024-51745-4

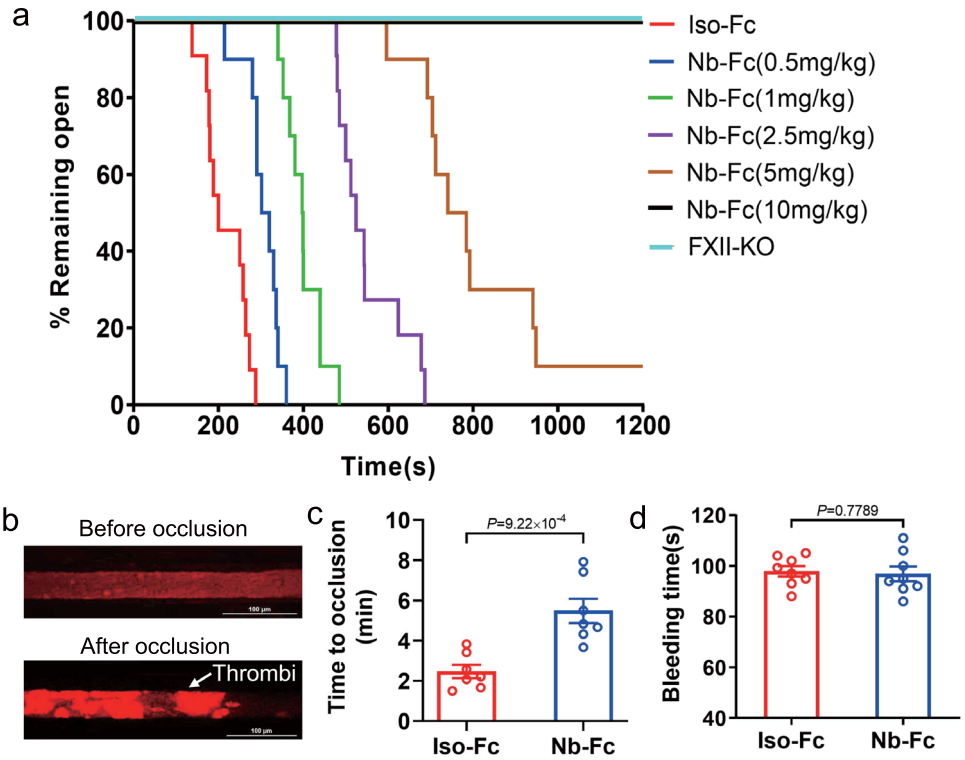


**Fig. 2 | Treatment with Nb-Fc inhibits thrombosis without affecting hemostasis in mice. a** Nb-Fc inhibited 7.5% $FeCl_3$-induced carotid arterial thrombosis. C57BL/6J mice were intraperitoneally injected with Nb-Fc or isotype control, Iso-Fc ($n = 7–11$), and *F12*$^{-/-}$ mice were used as control ($n = 7$). Time to vascular complete occlusion was monitored. **b**, **c** Nb-Fc treatment inhibited cremaster arterial thrombosis. Mice were intraperitoneally injected with 1 mg/kg Nb-Fc. Subsequently, mice were injected intravenously with 2% rose bengal (dissolved in PBS, 50 mg/kg) and PE-conjuated anti-CD41 antibody (2 µg/mouse), followed by 565-nm laser illumination at the cremaster artery. Representative images of thrombus formation taken by intravital microscopy (**b**, scale bar: 100 µm). Time to complete occlusion in the presence of Nb-Fc or Iso-Fc (**c**, $n = 7$). **d** Nb-Fc treatment did not affect hemostasis in mice ($n = 8$). Tail bleeding time in mice treated with 10 mg/kg Nb-Fc or Iso-Fc. The mean ± SEM of all data points are shown (**c**, **d**). Unpaired two-sided Student's *t* test was used. Source data are provided as a Source Data file.

providing gas exchange with an artificial circuit and membrane. The benefit of ECMO is limited by its major complications, namely, thrombosis and systemic inflammation[22]. Mortality rates ranging from 30–70% are reported for ECMO patients[23]. Almost all of these patients develop a systemic inflammatory response syndrome[24]. Blocking FXIIa prevented thrombosis during ECMO in previous studies[5,7–9] and interfered with kininogen cleavage-mediated BK formation in vitro[5]. However, the effect of FXIIa inhibition on ECMO-related inflammation is unknown. We established a mouse model of ECMO with features comparable to human ECMO including deposition of fibrin, leukocytes, platelets, and red blood cells on oxygenator membranes (Supplementary Fig. 11). We analyzed the effect of coadministration of Nb-Fc (2.0 mg/kg) and heparin (400 U/kg) versus the current standard of care, heparin (400 U/kg) alone, on ECMO-related inflammatory responses in mice (Fig. 3a). Nb-Fc treatment or FXII knockout substantially reduced thrombus deposition on oxygenator membranes (Fig. 3b) and total protein content on the oxygenator membranes in mice that underwent ECMO for 2 h (Fig. 3c). The presence of Nb-Fc or FXII deficiency also reduced microvascular thrombi in liver and kidney at 24 h after ECMO (Fig. 3d), without affecting ACT (Supplementary Fig. 12). Compared to baseline, connection to the ECMO circuit increased circulating levels of D-dimer, alkaline phosphatase, creatinine and TNF-α, at 24-h after ECMO, whereas treatment with Nb-Fc, on top of heparin (the standard treatment for human ECMO), significantly attenuated these pathological responses (Fig. 3e–h). Furthermore, intravital imaging of the microcirculation by spinning-disc confocal microscopy revealed that ECMO process triggered neutrophil adherence, platelet aggregation and neutrophil-platelet aggregation and that FXII knockout or Nb-Fc treatment attenuated these vascular inflammatory responses (Fig. 3i–m). Therefore, FXII blockade suppressed both artificial membrane-induced thrombosis and systemic microvascular thrombosis, and also ameliorated systemic inflammation, ultimately preventing organ damage without affecting hemostasis during ECMO.

### Nb-Fc inhibits immune induced local vasculitis in mice

We next explored a role of FXII in a second model of vascular inflammation, which is without artificial materials (as seen with ECMO). Vasculitis is an inflammatory disease that affects the vessel wall and leads to its compromise or destruction and subsequent hemorrhagic and ischemic events[25]. We firstly used a murine model of immune complex-mediated local vasculitis to examine the role of FXII. Nb-Fc treatment of wild-type significantly reduced the area of inflamed skin and the extent of hemorrhage as indicated by the amount of skin hemoglobin (Fig. 4a–c). Similar protection was also seen in FXII deficient mice. Histological staining of the affected skin revealed that neutrophil infiltration and myeloperoxidase (MPO) levels were substantially reduced in Nb-Fc treated or FXII deficient mice (Fig. 4d–g). Neutrophil depletion reduced vascular leakage in this model (Supplementary Fig. 13), confirming a critical role of neutrophils in vasculitis. These data suggest that Nb-Fc interferes with a mechanism related to neutrophil activities.

### Nb-Fc ameliorates anti-neutrophil cytoplasmic antibody-associated systemic vasculitis in mice

To further examine the impact of targeting FXII in vasculitis, we next utilized a model of anti-neutrophil cytoplasmic antibody (ANCA)-associated systemic vasculitis. The ANCA associated systemic

https://doi.org/10.1038/s41467-024-51745-4

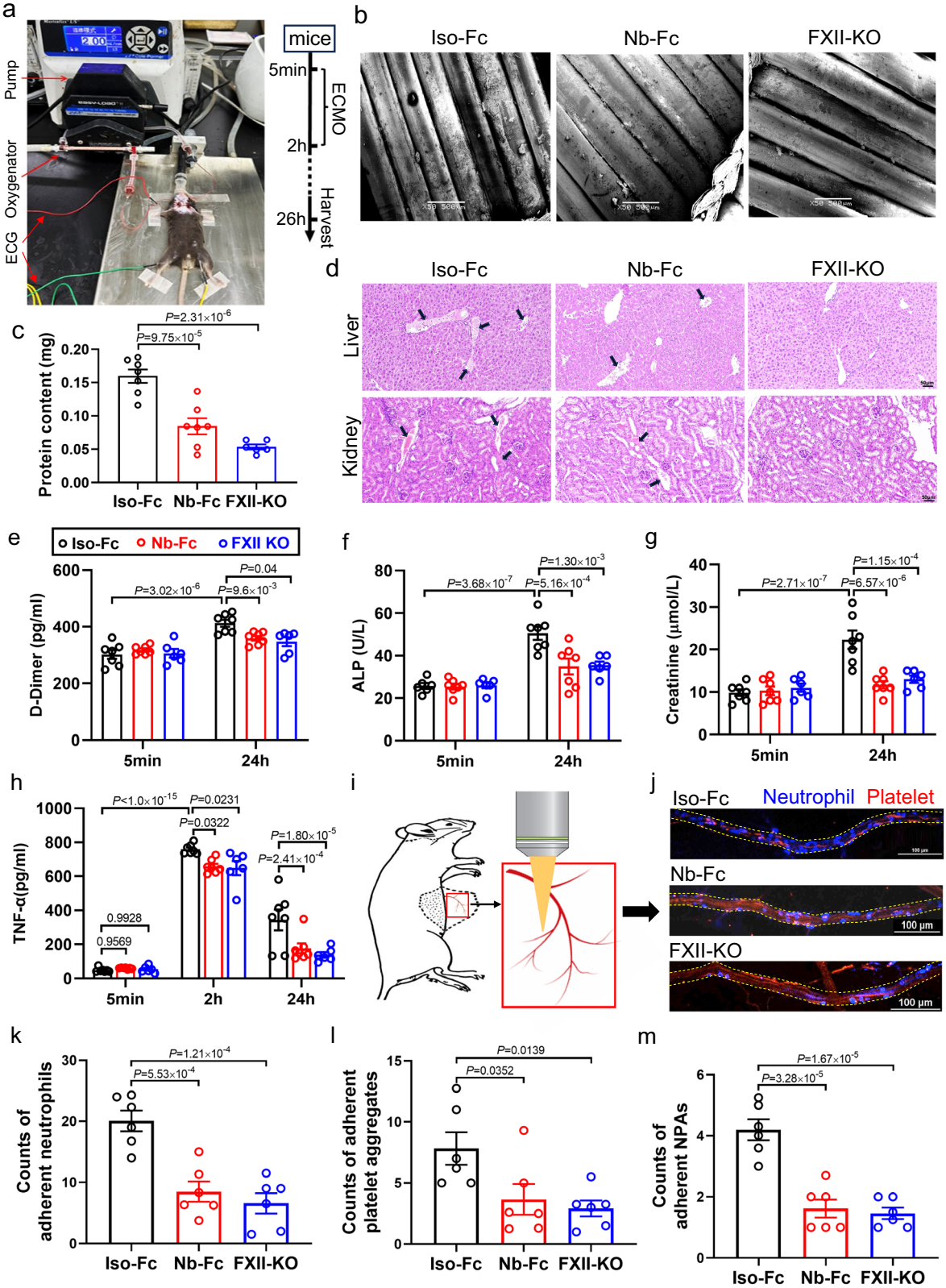


vasculitis is an autoimmune disease characterized by systemic inflammation and subsequent destruction of small to medium blood vessels within target organs, particularly the kidney, as seen in myeloperoxidase (MPO)-ANCA glomerulonephritis[26]. MPO-ANCA glomerulonephritis induction resulted in segmental glomerular necrosis and crescents in glomeruli. Wild type and FXII KO mice were immunized with mouse MPO on day 0 and day 7, followed by anti-glomerular basement membrane globulin challenge on day 15. Levels of anti-MPO antibody were similarly across these groups as examined on day 14 (Supplementary Fig. 14). Nb-Fc and control antibody were started to administer to wild type mice on day 15. Mice in the control group developed glomerular segmental glomerular necrosis and crescents in kidney, hallmark of ANCA glomerulonephritis. Nb-Fc treatment attenuated segmental glomerular necrosis and reduced formation of

https://doi.org/10.1038/s41467-024-51745-4

**Fig. 3 | FXII knockout or inhibition with Nb-Fc suppresses ECMO-related thrombosis and inflammation and ameliorates organ injury in mice.** **a** Photographic illustration of the mouse ECMO setup and the experimental procedure ECMO. The Iso-Fc group and the Nb-Fc group were both treated with heparin (400 U/kg). The Nb-Fc group also received coadministration of Nb-Fc (2 mg/kg), and FXII knockout mice were used as positive control, which were intravenously injected with heparin (400 U/kg) ($n = 6, 7$). **b** Oxygenator membranes of mouse ECMO were analyzed by scanning electron microscopy (SEM), scale bar: 500 μm. **c** Protein content on oxygenator membranes ($n = 6, 7$). **d** Representative pictures from H&E staining of liver or kidney. Arrows indicate areas with thrombi, scale bar: 50 μm. Plasma D-dimer (**e**), ALP (**f**), creatinine (**g**) of mice underwent 5-min ECMO (baseline) or mice after 24-h ECMO ($n = 6, 7$). **h** Plasma TNF-α of mice underwent 5-min or 2-h ECMO (baseline), and mice after 24-h ECMO ($n = 6, 7$). **i** Schematic of the mouse microcirculation detection by spinning disk confocal microscopy. After 24-h ECMO, the mice were anesthetized with pentobarbital sodium, BV421-anti-Ly6G antibody (2 μg/mouse) and PE-anti-CD41 antibody (2 μg/mouse) was injected to the mice intravenously. The abdominal skin was cut along the midline of the abdominal cavity. The abdominal skin (inside side up) was placed on the stage of the spinning disk confocal microscope. The adherent neutrophils (blue), platelet aggregates (red) or neutrophil-platelet aggregates (NPAs, blue & red) in the venules were detected by spinning disk confocal microscopy. **j** Representative pictures of adherent neutrophils, platelet aggregates and NPAs in venules. Scale bar: 100 μm. Counts of adherent neutrophils (**k**), platelet aggregates (**l**), NPAs (**m**) in venules ($n = 6$). Data are shown as mean ± SEM. One-way ANOVA with Dunnett's multiple comparisons test (**c**, **k**–**m**). Two-way ANOVA with Sidak's multiple comparisons (**e**–**h**). Source data are provided as a Source Data file.

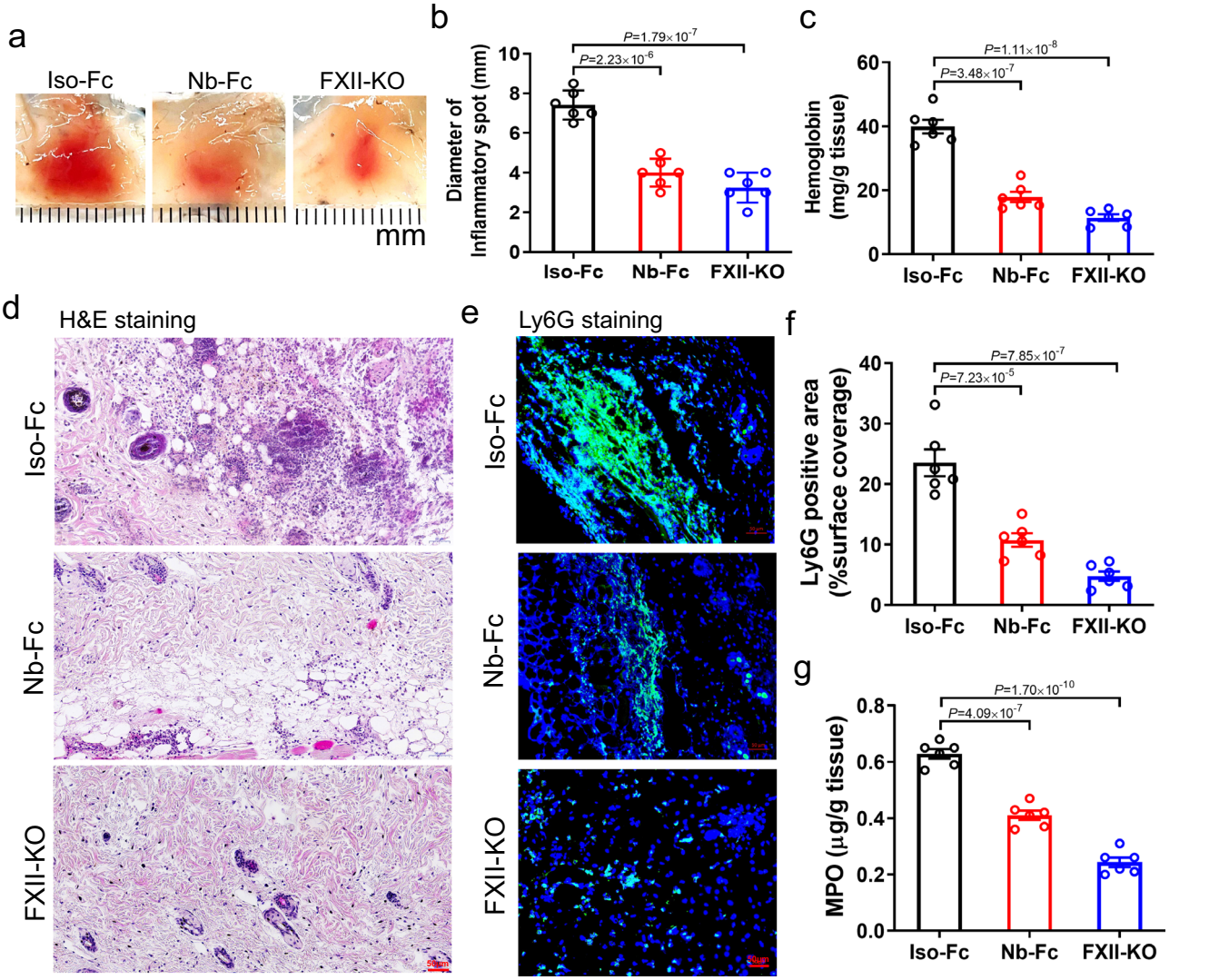


**Fig. 4 | FXII knockout or inhibition with Nb-Fc ameliorates immune complex-mediated vasculitis in mice.** **a** Representative macroscopic findings of hemorrhage in ICV mice. Wildtype mice were intraperitoneally injected with Nb-Fc or Iso-Fc (2 mg/kg), and FXII knockout mice were used as positive control. After 30 min, the mice were subjected to BSA (75 μg/g) and anti-BSA antibody (60 μg/mouse). Skin tissues were harvested four hours post BSA and anti-BSA antibody treatment ($n = 6$). **b** Diameter of the skin hemorrhage spots ($n = 6$). **c** Quantification of tissue hemoglobin levels by ELISA ($n = 6$). **d** H&E staining and **e** immunofluorescence staining of the dermal hemorrhage spots using an antibody specific for Ly6G (marker for neutrophils). Scale bar: 50 μm. **f** Quantification of Ly6G positive (green) areas ($n = 6$). **g** The MPO contents of mice in each group ($n = 6$). Data are presented as mean ± SEM. One-way ANOVA Dunnett's multiple comparisons test (**b**, **c**, **f**, **g**) was used. Source data are provided as a Source Data file.

https://doi.org/10.1038/s41467-024-51745-4

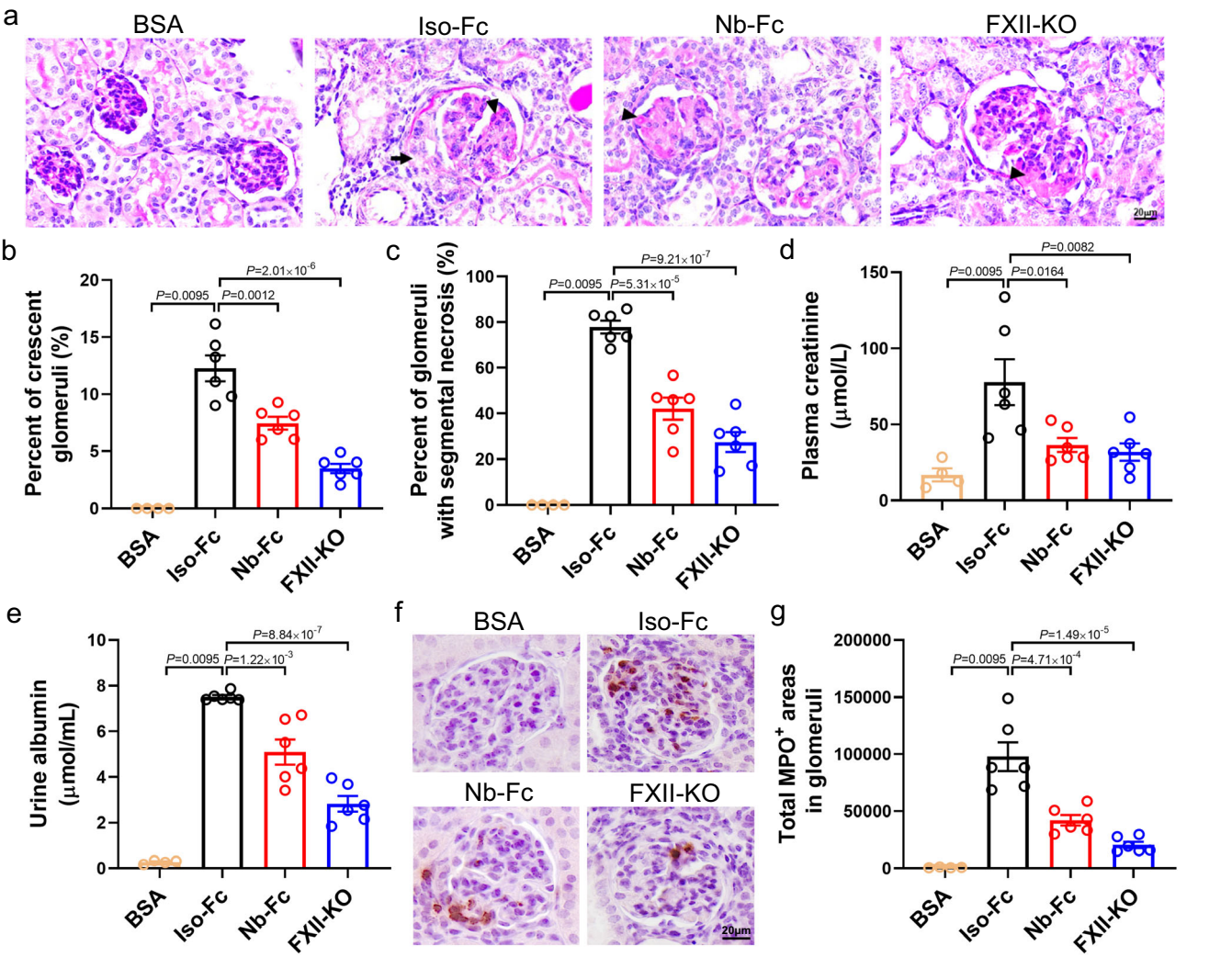


**Fig. 5 | FXII knockout or inhibition with Nb-Fc ameliorates ANCA associated systemic vasculitis in mice.** Mice were immunized with mouse myeloperoxidase (MPO, 20 μg/mouse) on day 0, 7, respectively ($n = 6$), and mice immunized with BSA were used as negative control ($n = 4$). Nb-Fc or Iso-Fc was administered to the mice at dose of 2 mg/kg at day 15, followed by injecting 500 μL anti-Glomerular Basement Membrane globulin to induce glomerulonephritis. FXII KO mice were used for comparison ($n = 6$). Blood, urine, and kidneys of the mice were collected on day 21. **a** Periodic acid Schiff staining of the kidney tissue. The arrow indicates crescent and arrow head indicates segmental necrosis. Scale bar: 20 μm. **b** Quantification of glomerular crescents. **c** Quantification of segmental glomerular necrosis (defined by positive PAS-staining with hypocellularity). **d**, **e** Concentrations of plasma creatinine and urinary albumin ($n = 4, 6$). **f** Immunohistochemistry staining of the kidney tissue. Scale bar: 20 μm. **g** Total MPO positive ($MPO^+$) areas in glomeruli of each cross-section ($n = 4, 6$). Data are presented as mean ± SEM. Non-parametric test with two-sided Mann–Whitney U test was used to compare the statistical difference between the BSA group and Iso-Fc group, and one-way ANOVA with Dunnett's multiple comparisons test was used to compare statistical difference among Iso-Fc group, Nb-Fc group, and FXII-KO group (**b**–**e**, **g**). See the Methods for details. Source data are provided as a Source Data file.

crescents (Fig. 5a–c). It also reduced plasma creatinine and urine albumin (Fig. 5d, e). Furthermore, Nb-Fc inhibited neutrophil accumulation in glomeruli (Fig. 5f, g). Deletion of FXII conferred similar protection as seen with Nb-Fc. Taken together, these data suggest that FXII inhibition or deletion ameliorated vasculitis, likely involving neutrophils.

### Impaired neutrophil migration by FXII inhibition

To delineate a potential direct action of FXII on neutrophils, which might underlie the above in vivo observations, we assessed neutrophil migration in vivo and in vitro. Nb-Fc treatment inhibited neutrophil chemotaxis to the peritoneal cavity following thioglycolate induction in mice (Fig. 6a–c). The effects of Nb-Fc treatment were seen as marked reductions of the total migrated cells/peritoneal exudative cells and neutrophils ($CD11b^+Ly6G^+$) in peritoneal lavage fluid. In addition, we assessed migration of total blood leukocytes in vitro by a transwell assay. Incubation with Nb-Fc selectively impeded migration of mouse neutrophils ($CD11b^+Ly6G^+$) and human neutrophils ($CD45^+CD16^+CD11b^+$) among total blood leukocytes (Fig. 6d–i).

### Nb-Fc inhibits thrombosis and neutrophil activation in human blood microfluidic analysis

Thrombosis involves platelet activation and coagulation and interacts with inflammation. Activation of FXII can be initiated upon contact with negatively charged surfaces, which can be either artificial (e.g., ellagic acid and kaolin) or of natural origin (e.g., collagen)[27]. We next investigated the effect of Nb-Fc on thrombo-inflammation under shear flow conditions using ex vivo human blood microfluidic assay (Fig. 7a). Perfusion of recalcified whole blood over collagen-coated slide surface resulted in robust formation of thrombi, consisted of platelet aggregates, fibrin, and neutrophils, accompanied with increase of

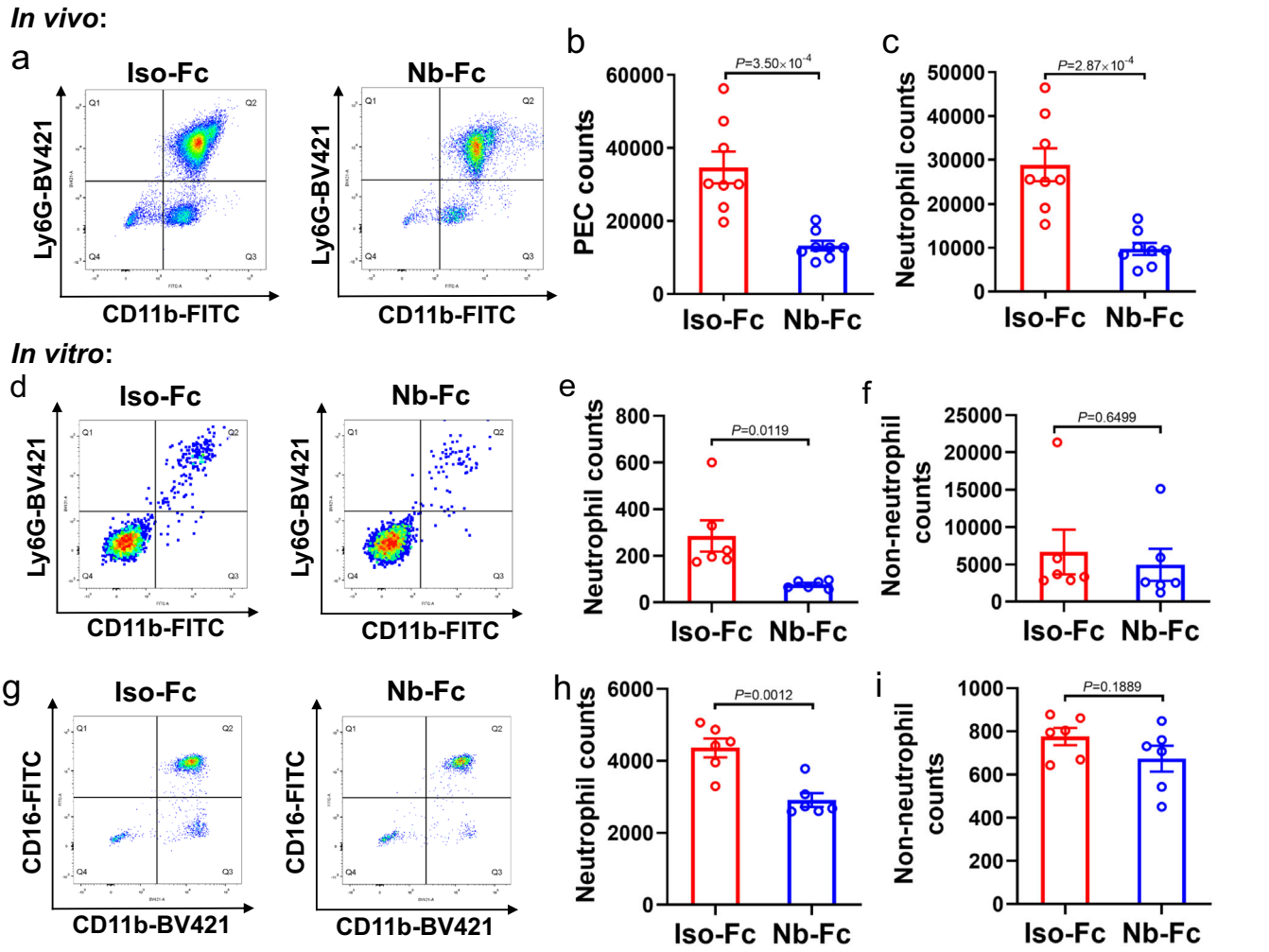


**Fig. 6 | Treatment with Nb-Fc selectively inhibits neutrophil migration. a–c** Nb-Fc supressed neutrophil migration in vivo. Mice were intraperitoneally injected with Nb-Fc or Iso-Fc, followed by injecting thioglycolate. The peritoneal lavage fluid was collected 4 h after injection. Flow cytometry was used to analyze cell types in the peritoneal lavage fluid. $Ly6G^+CD11b^+$ cells were identified as neutrophils. **a** Representative flow cytometric plots of peritoneal exudate cells (PECs) stained with antibodies against Ly6G and CD11b. Quantification of PECs (**b**, $n = 8$) and neutrophils (**c**, $n = 8$) in the peritoneal lavage fluid. **d–i** Nb-Fc inhibited neutrophil migration in vitro. White blood cells (WBCs) from were isolated from human and murine whole blood and used for migration assessment by transwell assay analysis. WBCs were placed in the upper chamber, followed by adding Nb-Fc or Iso-Fc (50 μg/mL). fMLP (2 μM) was added in the lower chamber to induce neutrophil migration. The migrated neutrophils in lower chamber were measured by flow cytometry. Representative flow cytometric plots of (**d**) murine and (**g**) human WBCs in the lower chamber of transwell. Counts of mouse neutrophils ($Ly6G^+CD11b^+$, **e**) and human neutrophil ($CD45^+CD16^+CD11b^+$, **h**) in lower chamber ($n = 6$). Counts of (**f**) mouse or (**i**) human cell types other than neutrophils (non-neutrophil leukocytes) in lower chamber ($n = 6$). Data are presented as mean ± SEM. Unpaired two-sided Student's $t$ test was used (**b**, **c**, **e**, **f**, **h**, **i**). Source data are provided as a Source Data file.

fibrinopeptide A (FPA) in the effluent from the slide chamber, while treatment with Nb-Fc, as compared with the isotype-control antibody, reduced surface-deposition of platelet aggregates, fibrin, and neutrophils, and FPA in the effluent (Fig. 7b–f). Furthermore, neutrophils ($CD45^+CD16^+CD11b^+$) in the effluent of the control group were activated, as indicated by increased surface expression of CD11b and LFA-1, while Nb-Fc treatment significantly suppressed neutrophil activation (Fig. 7g–j). Thus, Nb-Fc bears a promise to inhibit both thrombosis and inflammation in disease.

## Discussion

The present study demonstrates that FXII critically mediates the inflammatory responses in ECMO and vasculitis, at least partially via activating neutrophils.

We identified a single-domain antibody against FXII, which recognizes a conformational epitope involving the FnII and Kringle domains of the FXII heavy chain. Notably, the FnII domain constitutes the binding site of FXII for negatively charged surfaces[28], and an epitope within the amino-terminal 28 amino acids of FXII is associated with FXII activation[29]. A peptide fragment from FnII blocks FXII binding to endothelial cells and inhibits FXIIa's activation of FXI and prekallikrein[30]. FnII mediates the FXII binding to the globular C1q receptor (gC1qR) to form a complex that may initiate the intrinsic coagulation and bradykinin generation[31]. FnII is also reported to ensure FXII zymogen quiescence in vitro[32]. The Kringle domain involves in FXII activation, because a mutation in this domain accelerated FXII activation in vitro[33]. Intra-molecular interactions between FnII, Kringle and catalytic domains are also predicted[34]. Taken together, our data and these previous observations support that FnII and Kringle are important for physiological activation of FXII. The exact mechanism of action warrants future study.

Although the concept of targeting FXII for inflammatory disorders is emerging[1], its relevance to clinical scenarios is unclear. Previous antibodies against FXII/FXIIa[5–8] were reported to block coagulation/

https://doi.org/10.1038/s41467-024-51745-4

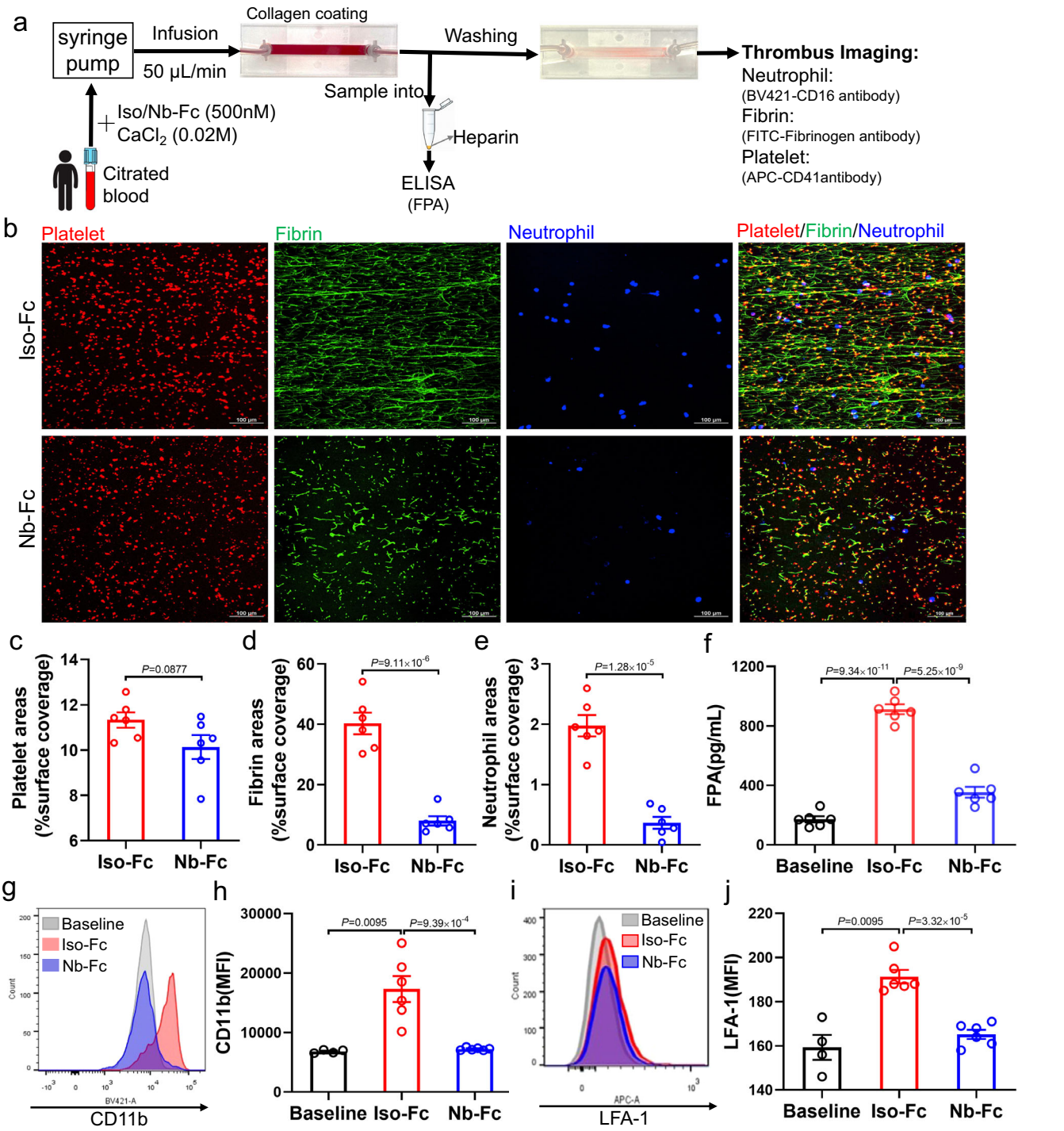


**Fig. 7 | Nb-Fc inhibits thrombus formation and neutrophil activation in human blood microfluidic analysis.** The microfluidic channel slides were coated with collagen (150 μg/mL). Citrated blood human blood was incubated with Nb-Fc or Iso-Fc at concentration of 500 nmol/L. Then, the blood was infused into channel slides with a velocity of 50 μL/min. The effluent of the flow device was collected for the detection of fibrinopeptide A (FPA) and neutrophil detection. Flow cytometery was used to measure the expressions of CD11b and LFA-1 on neutrophils. The thrombi in the channel slides were detected by spinning disk confocal microscopy using FITC conjugated anti-human fibrinogen antibody, APC conjugated anti-human CD41 antibody and BV421 conjugated anti-human CD16 antibody ($n = 6$). **a** Schematic of the microfluidic thrombosis assay. **b** Representative pictures of thrombi in collagen-coated channel slides. Scale bar: 100 μm. Quantification of CD41 positive areas (platelet, red, **c**), fibrin positive areas (green, **d**), CD16 positive areas (neutrophil, blue, **e**) in four randomly selected fields of each slide ($n = 6$). **f** The plasma FPA level in effluent ($n = 6$). Flow cytometry plots (**g**), and mean fluorescence intensity (MFI) of CD11b on neutrophils (**h**, $n = 4, 6$). Flow cytometry plots (**i**), and MFI of LFA-1 on neutrophils (**j**, $n = 4, 6$). Data are presented as mean ± SEM. Unpaired two-sided Student's $t$ test (**c**–**e**), one-way ANOVA with Dunnett's multiple comparisons test (**f**), and unpaired two-sided Student's $t$ test & two-sided Mann–Whitney U test (**h**, **j**) were used. Source data are provided as a Source Data file.

thrombosis and high molecular weight cleavage and interfere with bradykinin release and tissue swelling in patients with HAE type III[12] (these patients lack cardinal features of inflammation). Taking advantage of the discovered FXII inhibitor, Nb-Fc, we evaluated its efficacy in two animal models of vascular inflammation that are clinically relevant.

Systemic inflammation is a major cause of multi-organ failure and the high mortality (30–70%) in ECMO patients[22,23]. Contact activation of blood components with artificial surfaces and shear stress in the ECMO circuit can all contribute to the inflammatory responses. Although anti-thrombotic action of FXII inhibition during ECMO is well documented, its impact on ECMO-related inflammatory responses had been unknown[5,7–9]. Here, using a murine model of ECMO, both Nb-Fc treatment and FXII deletion substantially inhibited release of TNF-α, the prototype pro-inflammatory cytokine. Neutrophil adherence to microvascular endothelium was also reduced following FXII blockade. The ECMO-related inflammation is in line with FXII-dependent contact activation and neutrophil activation (Fig. 6, and below discussion). It is worthy to note that heparin, the standard anti-thrombotic medicine used in ECMO, suppresses activation of multiple coagulation factors, including thrombin, FX and FXI, but it also paradoxically activates FXII in a charge dependent manner[35]. The observed anti-inflammatory efficacy of Nb-Fc, which was administered on top of heparin, may reflect inhibition of FXII activation on ECMO-oxygenator and tubing and inhibition of heparin mediated FXII activation, suggesting a therapeutic opportunity over the current therapy with heparin.

The role of FXII in inflammation was also revealed in mouse models of immune complex-mediated local vasculitis and ANCA associated/anti-GBM-dependent vasculitis, which has no artificial surface-contact activation involved. FXII inhibition or its gene deletion attenuated the immune-induced local vasculitis and ameliorated ANCA associated systemic vasculitis. This is consistent with an impaired neutrophil migration both in vitro and in vivo following FXII inhibition (Fig. 6). Genetic deficiency of FXII impaired neutrophil migration via intracellular Akt2-$\alpha_M\beta_2$ integrin signaling, an effect attributable to neutrophil-expressed zymogen FXII, but not FXIIa[13]. The present study suggests a mechanism of action that *exocellular* interception with Nb-Fc can block FXII-mediated neutrophil migration, thus underlying the suppressed vascular inflammation. FXIIa dependent bradykinin formation might also contribute to the pathology of vasculitis[36], and leukocyte kinin B1 may play a role in ANCA associated GN by modulating neutrophil–endothelial interaction[37]. In human blood microfluidic analysis, Nb-Fc inhibited neutrophil adherence and activation, reducing expression of CD11b and LFA-1 (Fig. 7). In this context, FXII-dependent neutrophil activation might function synergistically with FXIIa mediated bradykinin formation.

Therefore, beyond its known effect in thrombosis, FXII critically mediates the inflammatory responses to the blood contact with foreign material (ECMO) and to the contact-free immune stimulation (vasculitis), which is mechanistically attributable to FXII dependent neutrophil activation. The function of FXII in these inflammatory diseases/conditions is schematically illustrated in Supplementary Fig. 15.

In summary, we report an alpaca-derived single-domain antibody (Nb-Fc) that inhibits FXII activation and show that FXII deletion or inhibition exhibits remarkable anti-inflammatory and antithrombotic effects. Nb-Fc, bears a promise for potential treatments of ECMO-related inflammation and vasculitis and of thromboembolic disease, without affecting hemostasis. Therapeutic exploration of FXII intervention for other diseases with inflammation as an essential pathology, such as myocardial ischemia and reperfusion, as we recently shown[38,39] warrants future investigation. Case reports and smaller clinical studies have associated low FXII with abortion. However, FXII levels are measured via an aPTT based assay in patients. Lupus anticoagulants is a strong risk factor for abortion and -similarly to FXII deficiency- prolongs the aPTT. Thus, the notion that low FXII is a risk factor for abortion might be biased by (undetected) Lupus anticoagulants cases. FXII null mice have normal pregnancy and do to show abortion.

## Methods

### Preparation of Nb and its construct Nb-Fc

800 μg of human FXII zymogen (Enzyme Research Laboratories) isolated from human plasma was emulsified with Freund's complete adjuvant (Millipore Sigma) and used for subcutaneous immunization of an alpaca. The animal was then immunized with FXII (400 μg) plus Freund's incomplete adjuvant at 21, 35 and 49 days after the initial immunization. Blood was collected 7 days after the last immunization, and lymphocytes were isolated from venous blood by density gradient centrifugation using Alpaca Peripheral Blood Lymphocyte Separation Solution (Beijing Baiaolaibo Technology Co., Beijing, China). Total RNA was extracted with the use of TRIzol reagent (Thermo Fisher Scientific). cDNA was synthesized by reverse transcription PCR (Takara) using Oligo dT. VHH sequences were amplified by nested PCR using previously published primers[40,41]. The VHH DNA was then ligated into the phagemid vector pHEN1. The recombinant phagemids were introduced into *E. coli* TG1 competent cells to construct a VHH library. The resulting library had ~$2.4 \times 10^8$ clones. 24 clones from the library were randomly selected to estimate the VHH insert ratio in the phagemid within the library by PCR. Another 20 clones from the library were randomly selected for DNA sequencing to monitor the library diversity. A representative aliquot of the library was cultured and infected with helper phage M13KO7 (New England Biolabs) to produce M13 phage particles decorated at their tip with the VHH during an overnight incubation at 37 °C with shaking at 220 rpm. Then the phage particles were purified from the culture supernatant with 1/5 volume of 20% polyethylene glycol 8000, 2.5 M NaCl solution at 4 °C for 4 h, then centrifuged at 12,000 × *g* at 4 °C for 10 min. The pellets were gently resuspended in 1 mL PBS, constituting the phage display library. Then the FXII specific VHHs were enriched from the phage displayed library using magnetic beads-based semi-automated bio-panning strategy. The binding activity to FXII of eluted phage particles from bio-panning was assessed by phage-ELISA using FXII coated plates. The VHH nucleotide sequences of the positive phage clones were then determined by DNA sequencing. VHH coding sequences for the positive phage clones were cloned into pET26b with an NcoI-XhoI seamless cloning kit (Tsingke Biotechnology Co., Ltd.). The selected VHH (Nb) and its isotype control (Iso), in which CDR1/2 and CDR3 were replaced respectively by 2 and 3 repeats of the GGGGS-linker sequence, were fused with an Fc segment of human immunoglobulin G4, and the corresponding sequences (Nb-Fc and Iso-Fc) were cloned into pcDNA3.4 vector. The recombinant pcDNA3.4 plasmids were used to transfect Chinese Hamster Ovary (CHO) cells (Thermo Fisher Scientific Inc., catalog NO.: R80007) for protein expression. Cells were grown in serum-free medium at 37 °C for 5 days to express recombinant protein. Nb-Fc antibody and its isotype control (Iso-Fc) were purified using AKTA purifier (GE Healthcare) using protein A medium. See detailed description in the supplementary method.

### In vitro assay of FXII activation

The method was based on a previous study[5], with a final reaction volume of 200 μl. Nb or Nb-Fc at different concentrations was incubated with FXII (5 μg/ml, final) in Nunc immuno-plates in a volume of 140 μL for 30 min at 37 °C. Ellagic acid (aPTT reagent, from Sysmex, consisting of ellagic acid and cephalin, 4 μg/mL), poly-phosphate (Millipore Sigma, type 65, 20 μg/mL) and dextran sulfate (Millipore Sigma, 500,000 Da, 2 μg/mL), were added in a volume of 20 μL, and the plate was further incubated at 37 °C for 10 min. Then, 40 μL S-2302 substrate (Chromogenix) was added to a final concentration of 0.8 mM and the plate was incubated at 37 °C for another 15 min. The reaction

was stopped by adding 40 µL of 20% acetic acid and the absorbance was measured at 405 nm.

### In vitro assay of plasma prekallikrein activation

The method was based on a previous study[6]. Nb-Fc at different concentrations was incubated with 0.02 µg human FXII in a volume of 140 µL at 37 °C for 30 min, then, 1.0 µg plasma prekallikrein and 20 µL ellagic acid (concentration: 4 µg/mL) was added and incubated at 37 °C for 15 min, followed by adding 30 µL CS-31(02) (BIOPHEN) and additional incubation at 37 °C for 10 min. The assay volume was 200 µl prior to stopping the reaction by adding 40 µL of 20% acetic acid. The change in absorbance was detected at 405 nm with a plate reader.

### Human blood coagulation assay

Antibodies at different concentrations were incubated with 60 µl human plasma (3.2% sodium citrate) from healthy donors in a final volume of 120 µL at 37 °C for 30 min. Then activated partial thromboplastin time (aPTT) was measured using an SF-400 semi-automatic coagulometer (Beijing Success Technology Inc., China), according to the manufacturer's instructions. Participants involved in the study were all healthy males between the ages of 25 and 35 years. One reason for only using blood from male individuals was to avoid potential menstruation-related effects. Written and informed consent was obtained from each participant. The studies using human whole blood complied with all relevant ethical regulations. Ethical approval was obtained from the Institutional Review Board, Fuwai Hospital, National Center for Cardiovascular Diseases, China.

### Mouse model of ECMO

The ECMO system consists of a peristaltic pump (Model 77200-60, Masterflex) with supporting silicone tubing, a custom-made small-volume oxygenator (Xi'an Xijing Medical Appliance Co., Ltd, China) with 60 $cm^2$ gas exchange area and the priming volume of silicone and oxygenator is ~500 µL. The entire circuit was primed with 500 µL of 6% hydroxyethyl starch (HES, Fresenius Kabi, USA) containing heparin (Shenggong Bioengineering (Shanghai) Co., LTD, China) at a concentration of 1 U/mL.

ECMO studies in mice were performed according to a previously published protocol with minor modifications[47]. In brief, male C57BL/6J mice (~30 g, Beijing Vital River Laboratory Animal Technology Co., Ltd.) were intravenously injected with heparin (400 U/kg) combined with Nb-Fc (2 mg/kg) or heparin (400 U/kg) combined with an isotype control antibody (Iso-Fc, 2 mg/kg). As a positive control, male FXII knockout mice (~30 g) of C57BL/6J background were intravenously injected with heparin (400 U/kg). Mice were initially anesthetized by inhaling 3.0% isoflurane mixed with air. The left and right jugular veins were exposed by making a lateral skin incision of 4 mm on the left side of the neck using fine scissors. The distal part was then ligated with an 8-0 silk suture using micro-forceps. A slip knot was placed at the proximal end of the vein. The anterior wall of the vein was incised using micro-scissors. A 2-Fr polyurethane (PU) cannula was inserted into the proximal part of the jugular vein, with slightly rotating to a depth of 4 cm, reaching the iliac bifurcation of inferior vena cava. A 1-Fr PU cannula was introduced to the right jugular vein and gently moved 5 mm towards the direction of right atrium. Secure the cannula with 8-0 silk knots using micro forceps. Insert Electrocardiogram (ECG) needles connected to a data acquisition device were inserted into both forelimbs and hindlimb. ECMO was initiated on the animal by turning on the pump with an initial flow rate of 0.5 mL/min, and the flow rate of the pump was adjusted to 2 mL/min within the next 5 min. 5 min after the initiation of ECMO, 250 µL blood was collected via an extra tube built in before the oxygenator, then the circuit was refilled with 250 µL 6% HES. After 2 h ECMO running, the flow rate was reduced on the pump gradually (over the course of 5 min), thereby stopping ECMO. 250 µL blood from circuit of silicone hose and oxygenator was flowed into the mouse, and the left blood was collected for measurement. The cannulas were removed from the mice, and the incisions were sewn up. Gentamicin (100 mg/kg) was injected intraperitoneally into the mice, then the mice were housed for 24 h. 24 h later, the mice were anesthetized with pentobarbital sodium, and BV421-anti-Ly6G antibody (2 µg/mouse, Biolegend) and PE-anti-CD41 antibody (2 µg/mouse, Biolegend) were injected intravenously into the mice. The abdominal skin was cut along the midline of the abdominal cavity and placed on the stage of the spinning disk confocal microscope (Nikon) with the inner side facing upwards. The adherent neutrophils, platelet aggregates or neutrophil-platelet aggregates (NPA) in the venules were detected by spinning disk confocal microscopy. 2-4 vessels with a diameter of 10-25 µm from each mouse were selected, and the numbers of adherent neutrophils, platelets and NPA in the vessels were counted. After spinning disk confocal microscopy analysis, the blood of the mice was collected from inferior vena cava, followed by harvest the organs of the mice.

### ECMO analysis

Two QUADROXOLS oxygenators (MAQUET Inc., Germany) from human ECMO (duration: 147 h and 160 h, both patients survived) were collected. After decannulation, mouse ECMO oxygenator membranes were washed with 100 mL PBS, and human ECMO oxygenator membranes were washed with 2000 mL PBS, then fixed with 2.5% glutaraldehyde (Millipore Sigma). Five pieces (1 cm × 1 cm), taken from the four corners and the center of each membrane, were analyzed by scanning electron microscopy (SEM). The left oxygenator membrane was placed in 5 mL NaOH (1 M) solution and removed after 24 h. The protein concentration in the NaOH was measured by BCA (Thermo Fisher Scientific). The cells adhering to the oxygenator membrane were analyzed by immunofluorescence staining. TNF-α and D-dimer plasma levels were measured for each group using a TNF-α and D-dimer ELISA kit (Elabscience Biotechnology Co., Ltd, China), respectively. An automated biochemical analyzer (FUJIFILM Corporation) was used to measure plasma levels of alkaline phosphatase (ALP) and creatinine (Cre). Liver and kidney samples were fixed in 10% formalin, and embedded in paraffin. The fixed tissue was cross-sectioned at a thickness of 5 µm and stained with hematoxylin and eosin (H&E). Stained tissue sections were analyzed using the Pannoramic SCAN II system (3DHISTECH Ltd.).

### Mouse model of immune complex-mediated vasculitis (ICV)

Eight-week-old male C57BL/6J mice were administered 2 mg/kg Nb-Fc intraperitoneally. The mice were then anesthetized and the back skin was depilated. Thirty minutes after antibody administration, mice were injected intravenously with BSA (75 µg/g, Millipore Sigma). Immediately after BSA injection, 20 µL polyclonal rabbit anti-BSA IgG (60 µg, Millipore Sigma) was injected intradermally into the back skin. Four hours later, mice were sacrificed, and the skin around the injection site was removed at the level of fascia above skeletal muscle and was reversed as previously described[42].

To quantify the edema, the diameter on the fascial side of the ICV injection site was measured, and the diameter of the major and minor axis of the edema was averaged for analysis. To quantify hemorrhage, skins were grinded in RIPA buffer, and the hemoglobin content was measured by hemoglobin ELISA kit (Abcam).

To evaluate inflammatory cell infiltration, ICV tissue was fixed in 10% formalin and embedded in paraffin. Sections (5 µm thick) were stained with H&E. Anti-CD11b antibody (Abcam, 1:200) and anti-Ly6G antibody (Abcam, 1:200) were used for cell infiltration analysis by immunofluorescence. Another set of skin tissues was ground in RIPA buffer, and the MPO content was measured using an MPO ELISA kit (Abcam).

### Anti-MPO glomerulonephritis mouse model

To induce anti-MPO glomerulonephritis, 8-week-old male C57BL/6J and *F12*$^{-/-}$ mice were immunized subcutaneously on day 0 with 20 μg mouse myeloperoxidase (MPO; MedChemExpress) in Freund's Complete Adjuvant (Sigma-Aldrich). On day 7, mice received a booster subcutaneous injection of 20 μg MPO in Freund's Incomplete Adjuvant (Sigma-Aldrich). Plasma anti-MPO antibody titers of the immunized mice were measured on day 14. Briefly, wells of a 96-well ELISA plate were coated with 100 μL MPO (1 μg/mL in carbonate/bicarbonate buffer) per well. After blocking with 5% skim milk at 37 °C for 2 h, tested plasma was then added to each well, and incubated at 37 °C for 2 h. After washing with PBST (PBS plus 0.05% Tween 20), HRP-conjugated anti-mouse IgG (1:5000, Abcam) was added to each well and incubated for 1 h at 37 °C. After washing, tetramethylbenzidine (50 μL) was added to each well, then the reaction was stopped with 2 M $H_2SO_4$. The optical density (OD) was measured using an ELISA microplate reader at a wavelength of 450 nm. Nb-Fc or Iso-Fc was administered at dose of 2 mg/kg on day 15. MPO was deposited in the glomeruli by recruited neutrophils after 500 μL of Anti-Glomerular Basement Membrane Globulin (Probetex Inc. PTX-001) was injected intravenously to induce glomerulonephritis[43–45]. Urine was collected 24 h before the end of experiment. Mice were euthanized on day 21, and blood, kidneys, and spleens were collected. Levels of creatinine in plasma and albumin in urine were determined by Creatinine ELISA Kit and Albuminuria ELISA Kit (Elabscience Biotechnology Co., Ltd, China), respectively.

### Histologic evaluation of renal injury

Kidneys were fixed in 10% formalin, and embedded in paraffin. Cross sections (5 μm thickness) of specimens were stained with periodic acid–Schiff (PAS) and the entire tissue image was scanned by Pannoramic SCAN II (3DHISTECH Ltd., Hungary) for histological examination. Segmental glomerular necrosis and crescent glomeruli were assessed on PAS-stained sections. Necrosis area was defined as PAS-positive staining with hypocellularity. All glomeruli of each cross-section were evaluated, and the percentage of glomeruli with crescents or segmental glomerular necrosis was calculated. In addition, cross-sections of kidneys were stained with anti-MPO antibody (1:200, Abcam), followed by stained with HRP conjugated secondary antibody (1:100, Beijing Zhongshan Golden Bridge Biotechnology Co., Ltd.). After 3,3′-diaminobenzidine staining and counterstain with hematoxylin, the entire tissue image was scanned by Pannoramic SCAN II for histological examination. All glomeruli of each cross-section were evaluated. The MPO positive areas in glomeruli of each cross-section were analyzed by Image-Pro Plus software 6.0, and total MPO positive areas in glomeruli of each cross-section were summed. The pathology examinator was blinded to the treatment/grouping information.

All mice were housed under specific pathogen-free conditions in the animal facility at Fuwai Hospital. Standard rodent chow diet and water were available ad libitum. The facility was maintained at 22 ± 2 °C, with humidity of 55 ± 15%, and kept in a 12 h light–dark cycle. Male mice were used because potential menstruation-related effects could be avoided and their relatively larger body size made it easy for surgical operation with less stress to the animal. The animal protocols complied with relevant ethical regulations and were approved by the Institutional Animal Care and Use Committee, Fuwai Hospital, National Center for Cardiovascular Diseases, China.

### Microfluidic thrombo-inflammation assay

The microfluidic assay was based on a previous study[46]. The microfluidic system was consisted of a syringe pump (LongerPump), channel slide (μ-Slide I Luer, channel Height: 0.4 mm, Ibidi) and biocompatible silicone tubing (Inner Diameter: 0.8 mm, Ibidi). The channel slides were coated with collagen (150 μg/mL, HYPHEN BioMed) at 4 °C overnight. After removal of the coating solution, the channel slide was refilled with PBS before running the flow experiment. Fresh human blood was collected from healthy donors using sodium citrate anticoagulant tubes. Nb-Fc or Iso-Fc was firstly added in anticoagulant tubes with a working concentration of 500 nmol/L. Then 100 μL calcium chloride (0.2 M) was added to each of the above anticoagulant tubes. The blood was then immediately infused into channel slides by syringe pump at a constant flow rate of 50 μL/min, which corresponded to a velocity of 50 μL/min. Effluent from the flow chamber was collected into Eppendorf tubes with each containing 50 μL heparin (0.15 U/μL) for blood cell count and fibrinopepide A (FPA) detection. After 8 min, the blood infusion was stopped, and PBS was infused into the channel slides to wash the slides at a constant flow rate of 100 μL/min. After 20 min washing, the channel slides were blocked by 2.5% BSA (dissolved in PBS) for 30 min, followed by incubation with FITC conjugated anti-human fibrinogen antibody (1:100, Abcam), APC conjugated anti-human CD41 antibody (1:100, Biolegend) and BV421 conjugated anti-human CD16 antibody (1:100, Biolegend) at room temperature in dark for 10 min. Then the channel slides were washed with PBS, and the thrombi formed and adherent cells on the channel slides were visualized by a spinning disk confocal microscope (Nikon). Positively stained area was analyzed by Image Pro Plus 6.0, and mean of four randomly selected fields (200X) for each channel slide was used for comparison. The FPA in plasma of effluent was measured by ELISA according to the manufacturer's recommendations. The ELISA kit was purchased from Elabscience Biotechnology Co.,Ltd. Neutrophils in effluent were analyzed by flow cytometry using antibodies against CD45, CD16, CD11b, LFA-1 (1:50, Biolegend). $CD45^+CD16^+CD11b^+$ cells were identified as neutrophil, and the mean fluorescent intensity of CD11b and LFA-1 on neutrophils were analyzed.

### Statistics

Statistical analysis was performed using GraphPad Prism 8 software. For experiments with small sample size ($n < 6$), power calculations were not performed, and $P$ values were determined by non-parametric analysis. Other data were checked for normality before analysis by Shapiro–Wilk test. For all normally distributed data, an unpaired two-tailed Student's $t$ test was used for comparisons between two groups, one-way ANOVA with Tukey post hoc tests for comparisons between multiple groups, and two-way ANOVA (or two-way repeated-measures ANOVA) for comparisons between multiple groups when there were 2 experimental factors. If the data are not normally distributed or if n is too small to assess normality, Mann–Whitney U test was used for comparisons between two groups, and Dunn's multiple comparisons test for comparisons between multiple groups. IC50 calculations were analyzed by non-linear regression. Data were expressed as mean ± standard error of mean (SEM). Differences were considered statistically significant at $P < 0.05$.

Additional description of the methods is available in the supplemental information.

### Reporting summary

Further information on research design is available in the Nature Portfolio Reporting Summary linked to this article.

## Data availability

All data supporting the findings of this study are available within this paper and its Supplementary Information. Source data are provided with this paper.

## References

1. Maas, C. & Renné, T. Coagulation factor XII in thrombosis and inflammation. *Blood* **131**, 1903–1909 (2018).
2. Stavrou, E. & Schmaier, A. H. Factor XII: what does it contribute to our understanding of the physiology and pathophysiology of hemostasis & thrombosis. *Thromb. Res.* **125**, 210–215 (2010).

3. Renné, T. et al. Defective thrombus formation in mice lacking coagulation factor XII. *J. Exp. Med.* **202**, 271–281 (2005).
4. Kleinschnitz, C. et al. Targeting coagulation factor XII provides protection from pathological thrombosis in cerebral ischemia without interfering with hemostasis. *J. Exp. Med.* **203**, 513–518 (2006).
5. Larsson, M. et al. A factor XIIa inhibitory antibody provides thromboprotection in extracorporeal circulation without increasing bleeding risk. *Sci. Transl. Med.* **6**, 222ra217 (2014).
6. Matafonov, A. et al. Factor XII inhibition reduces thrombus formation in a primate thrombosis model. *Blood* **123**, 1739–1746 (2014).
7. Wallisch, M. et al. Antibody inhibition of contact factor XII reduces platelet deposition in a model of extracorporeal membrane oxygenator perfusion in nonhuman primates. *Res. Pr. Thromb. Haemost.* **4**, 205–216 (2020).
8. Wilbs, J. et al. Cyclic peptide FXII inhibitor provides safe anticoagulation in a thrombosis model and in artificial lungs. *Nat. Commun.* **11**, 3890 (2020).
9. Pireaux, V. et al. Anticoagulation With an Inhibitor of Factors XIa and XIIa During Cardiopulmonary Bypass. *J. Am. Coll. Cardiol.* **74**, 2178–2189 (2019).
10. Yau, J. W. et al. Selective depletion of factor XI or factor XII with antisense oligonucleotides attenuates catheter thrombosis in rabbits. *Blood* **123**, 2102–2107 (2014).
11. Fredenburgh, J. C., Gross, P. L. & Weitz, J. I. Emerging anticoagulant strategies. *Blood* **129**, 147–154 (2017).
12. Bjorkqvist, J. et al. Defective glycosylation of coagulation factor XII underlies hereditary angioedema type III. *J. Clin. Invest.* **125**, 3132–3146 (2015).
13. Stavrou, E. X. et al. Factor XII and uPAR upregulate neutrophil functions to influence wound healing. *J. Clin. Invest.* **128**, 944–959 (2018).
14. Gobel, K. et al. Blood coagulation factor XII drives adaptive immunity during neuroinflammation via CD87-mediated modulation of dendritic cells. *Nat. Commun.* **7**, 11626 (2016).
15. Hamers-Casterman, C. et al. Naturally occurring antibodies devoid of light chains. *Nature* **363**, 446–448 (1993).
16. Van Heeke, G. et al. Nanobodies® as inhaled biotherapeutics for lung diseases. *Pharmacol. Therapeutics* **169**, 47–56 (2017).
17. Muyldermans, S. A guide to: generation and design of nanobodies. *FEBS J.* **288**, 2084–2102 (2021).
18. Uchański, T., Pardon, E. & Steyaert, J. Nanobodies to study protein conformational states. *Curr. Opin. Struct. Biol.* **60**, 117–123 (2020).
19. Mazepa, M. A., Masias, C. & Chaturvedi, S. How targeted therapy disrupts the treatment paradigm for acquired TTP: the risks, benefits, and unknowns. *Blood* **134**, 415–420 (2019).
20. Heestermans, M. et al. Identification of the factor XII contact activation site enables sensitive coagulation diagnostics. *Nat. Commun.* **12**, 5596 (2021).
21. Zhang, Y. et al. Factor XII and prekallikrein promote microvascular inflammation and psoriasis in mice. *Br. J. Pharmacol.* (2024). doi: 10.1111/bph.16428.
22. Sniderman, J., Monagle, P., Annich, G. M. & MacLaren, G. Hematologic concerns in extracorporeal membrane oxygenation. *Res. Pr. Thromb. Haemost.* **4**, 455–468 (2020).
23. Granja, T. et al. Multi-Modal Characterization of the Coagulopathy Associated With Extracorporeal Membrane Oxygenation. *Crit. Care Med.* **48**, e400–e408 (2020).
24. Millar, J. E., Fanning, J. P., McDonald, C. I., McAuley, D. F. & Fraser, J. F. The inflammatory response to extracorporeal membrane oxygenation (ECMO): a review of the pathophysiology. *Crit. Care* **20**, 387 (2016).
25. Chen, K. R. & Carlson, J. A. Clinical approach to cutaneous vasculitis. *Am. J. Clin. Dermatol.* **9**, 71–92 (2008).
26. Shochet, L., Holdsworth, S. & Kitching, A. R. Animal Models of ANCA Associated Vasculitis. *Front. Immunol.* **11**, 525 (2020).
27. Smith, S. A. et al. Polyphosphate modulates blood coagulation and fibrinolysis. *Proc. Natl. Acad. Sci. USA* **103**, 903–908 (2006).
28. Citarella, F., te Velthuis, H., Helmer-Citterich, M. & Hack, C. E. Identification of a putative binding site for negatively charged surfaces in the fibronectin type II domain of human factor XII–an immunochemical and homology modeling approach. *Thrombosis Haemost.* **84**, 1057–1065 (2000).
29. Naudin, C., Burillo, E., Blankenberg, S., Butler, L. & Renné, T. Factor XII Contact Activation. *Semin. Thrombosis Hemost.* **43**, 814–826 (2017).
30. Mahdi, F., Madar, Z. S., Figueroa, C. D. & Schmaier, A. H. Factor XII interacts with the multiprotein assembly of urokinase plasminogen activator receptor, gC1qR, and cytokeratin 1 on endothelial cell membranes. *Blood* **99**, 3585–3596 (2002).
31. Kaira, B. G., et al. Factor XII and kininogen asymmetric assembly with gC1qR/C1QBP/P32 is governed by allostery. *Blood* **136**, 1685–1697 (2020).
32. Clark, C. C. et al. The Fibronectin Type II Domain of Factor XII Ensures Zymogen Quiescence. *Thrombosis Haemost.* **120**, 400–411 (2020).
33. Hofman, Z. L. M. et al. A mutation in the kringle domain of human factor XII that causes autoinflammation, disturbs zymogen quiescence, and accelerates activation. *J. Biol. Chem.* **295**, 363–374 (2020).
34. Frunt, R., El Otmani, H., Gibril Kaira, B., de Maat, S. & Maas, C. Factor XII Explored with AlphaFold - Opportunities for Selective Drug Development. *Thrombosis Haemost.* **123**, 177–185 (2023).
35. Oschatz, C. et al. Mast cells increase vascular permeability by heparin-initiated bradykinin formation in vivo. *Immunity* **34**, 258–268 (2011).
36. Kahn, R. et al. Contact-system activation in children with vasculitis. *Lancet* **360**, 535–541 (2002).
37. Hu, P. et al. Kinin B1 Receptor Is Important in the Pathogenesis of Myeloperoxidase-Specific ANCA GN. *J. Am. Soc. Nephrology* **31**, 297–307 (2020).
38. Zhu, L. et al. The cyclooxygenase-1/mPGES-1/endothelial prostaglandin EP4 receptor pathway constrains myocardial ischemia-reperfusion injury. *Nat. Commun.* **10**, 1888 (2019).
39. Wan, Q. et al. Targeting PDE4B (Phosphodiesterase-4 Subtype B) for Cardioprotection in Acute Myocardial Infarction via Neutrophils and Microcirculation. *Circulation Res.* **131**, 442–455 (2022).
40. Liu, X. et al. VHH phage-based competitive real-time immuno-polymerase chain reaction for ultrasensitive detection of ochratoxin A in cereal. *Anal. Chem.* **86**, 7471–7477 (2014).
41. Pleiner, T. et al. Nanobodies: site-specific labeling for super-resolution imaging, rapid epitope-mapping and native protein complex isolation. *eLife* **4**, e11349 (2015).
42. Aymé, G. et al. A novel single-domain antibody against von Willebrand factor A1 domain resolves leukocyte recruitment and vascular leakage during inflammation—brief report. *Arteriosclerosis Thrombosis Vasc. Biol.* **37**, 1736–1740 (2017).
43. Ooi, J. D. et al. A plasmid-encoded peptide from Staphylococcus aureus induces anti-myeloperoxidase nephritogenic autoimmunity. *Nat. Commun.* **10**, 3392 (2019).
44. Chang, J. et al. CD8+ T cells effect glomerular injury in experimental anti-myeloperoxidase GN. *J. Am. Soc. Nephrol.* **28**, 47–55 (2017).
45. Kumar, S. V. et al. Neutrophil extracellular trap-related extracellular histones cause vascular necrosis in severe GN. *J. Am. Soc. Nephrol.* **26**, 2399–2413 (2015).
46. Zhu, S., Chen, J. & Diamond, S. L. Establishing the transient mass balance of thrombosis: from tissue factor to thrombin to fibrin under venous flow. *Arteriosclerosis Thrombosis Vasc. Biol.* **38**, 1528–1536 (2018).

47. Madrahimov, N. et al. Veno-venous extracorporeal membrane oxygenation in a mouse. *J Vis Exp*. **140**, 58146 (2018).

## Acknowledgements

This work was supported by the National Key Research and Development Program of China [2023YFE0118800 to M.W.], the National Natural Science Foundation of China [82320108002 to M.W., 92149305 to D.L.], Chinese Academy of Medical Sciences (CAMS) Innovation Fund for Medical Sciences [2021-I2M-1-016, 2023-I2M-2-003, 2020-I2M-2-010, 2016-I2M-1-003, to M.W.], research funds from Fuwai Hospital [2022-GSP-GG-8 to M.W.] and the State Key Laboratory of Cardiovascular Diseases (2024GZZD-04 to M.W., 2024GZQN-05 to P.X.), and the Non-profit Central Research Institute Fund of CAMS [2023-PT310-03 to M.W.]. T.R. acknowledges the Deutsche Forschungsgemeinschaft (DFG, German Research Foundation) grants A11/SFB 877, B8/SFB 841 and P6/KFO 306. The authors thank Yonghu Huang (Fuwai Hospital), Qiaoni Zhang (Fuwai Hospital) for animal experiment and Guoli Yang (Zhejiang Normal University) for recombinant protein expression.

## Author contributions

M.W. conceived, supervised the study and wrote the paper. P.X. performed most of the experiments, analyzed the data and wrote the paper. Y.Z. contributed to eukaryotic expression, microfluidic experiments, and experiments of flow cytometry. J.G. contributed to the ECMO experiment and Anti-MPO glomerulonephritis experiment, H. L., H.R., P.Z. contributed to nanobody screening. H.L. contributed to mouse breeding and the migration experiment. L.C. and B.J. contributed to the ECMO experiment. Z.C. contributed to the histological evaluation. H.C. provided experimental assistance and advices. S.K. performed epitope mapping experiments and revised the manuscript. J.W., J.L., N.L., D.L. and T.R. provided study advices, interpreted the results, and/or critically revised the manuscript.

## Competing interests

M.W. is a co-founder of NINGBO COMGEN BIOTECH CO., LTD. The remaining authors declare no competing interests.

## Additional information

**Supplementary information** The online version contains supplementary material available at https://doi.org/10.1038/s41467-024-51745-4.

**Correspondence** and requests for materials should be addressed to Miao Wang.

**Peer review information** *Nature Communications* thanks Serge Muyldermans and the other, anonymous, reviewer(s) for their contribution to the peer review of this work. A peer review file is available.

**Reprints and permissions information** is available at http://www.nature.com/reprints

**Publisher's note** Springer Nature remains neutral with regard to jurisdictional claims in published maps and institutional affiliations.



[1]State Key Laboratory of Cardiovascular Disease, Fuwai Hospital, National Center for Cardiovascular Diseases, Chinese Academy of Medical Sciences and Peking Union Medical College, Beijing, China. [2]College of Life Science, Zhejiang Normal University, Jinhua, Zhejiang, China. [3]Institute of Clinical Chemistry and Laboratory Medicine, University Medical Center Hamburg-Eppendorf (UKE), Hamburg, Germany. [4]Synthetic and Functional Biomolecules Center, Beijing National Laboratory for Molecular Sciences, College of Chemistry and Molecular Engineering, Peking University, Beijing, China. [5]Department of Cardiopulmonary Bypass, State Key Laboratory of Cardiovascular Medicine, Fuwai Hospital, National Center for Cardiovascular Diseases, Chinese Academy of Medical Sciences and Peking Union Medical College, Beijing, China. [6]Renal Division, Peking University First Hospital, Beijing, China. [7]MOH Key Laboratory of Systems Biology of Pathogens, Institute of Pathogen Biology, Chinese Academy of Medical Sciences and Peking Union Medical College, Beijing, China. [8]Department of Medicine-Solna, Cardiovascular Medicine Unit, Karolinska Institute, Stockholm, Sweden. [9]Key Laboratory of Common Mechanism Research for Major Diseases, Department of Biochemistry and Molecular Biology, Institute of Basic Medical Sciences, Chinese Academy of Medical Sciences & Peking Union Medical College, Beijing, China. [10]Center for Thrombosis and Hemostasis (CTH), Johannes Gutenberg University Medical Center, Mainz, Germany. [11]Irish Centre for Vascular Biology, School of Pharmacy and Biomolecular Sciences, Royal College of Surgeons in Ireland, Dublin, Ireland. [12]Clinical Pharmacology Center, Fuwai Hospital, National Center for Cardiovascular Diseases, Chinese Academy of Medical Sciences and Peking Union Medical College, Beijing, China. [13]National Health Commission Cardiovascular Disease Regenerative Medicine Research Key Laboratory, Central China Subcenter of National Center for Cardiovascular Diseases, Henan Cardiovascular Disease Center, Fuwai Central-China Cardiovascular Hospital, Central China Fuwai Hospital of Zhengzhou University, Zhengzhou, China. [14]These authors contributed equally: Pengfei Xu, Yingjie Zhang. ✉e-mail: miao.wang@pumc.edu.cn